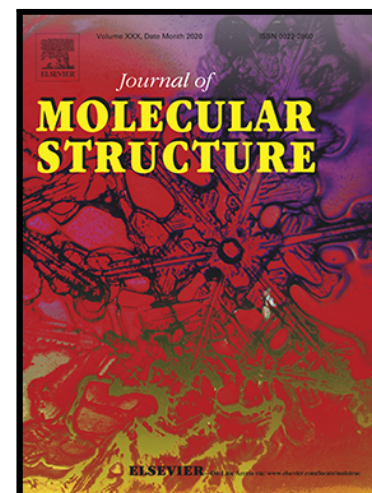


Journal Pre-proof

New Indolo[3,2-b]indole based small organic molecules for Organic Thin Film Transistors (OTFTs): A Combined Experimental and DFTStudy



Venkat Swamy Puli , Mahesh Subburu , Bhongiri Yadagiri ,
Anuj Tripathi , K.R.S. Prasad , Anindita Chatterjee ,
Someshwar Pola , Prabhakar Chetti

PII: S0022-2860(20)31806-8
DOI: <https://doi.org/10.1016/j.molstruc.2020.129491>
Reference: MOLSTR 129491

To appear in: *Journal of Molecular Structure*

Received date: 2 September 2020
Revised date: 17 October 2020
Accepted date: 18 October 2020

Please cite this article as: Venkat Swamy Puli , Mahesh Subburu , Bhongiri Yadagiri , Anuj Tripathi , K.R.S. Prasad , Anindita Chatterjee , Someshwar Pola , Prabhakar Chetti , New Indolo[3,2-b]indole based small organic molecules for Organic Thin Film Transistors (OTFTs): A Combined Experimental and DFTStudy, *Journal of Molecular Structure* (2020), doi: <https://doi.org/10.1016/j.molstruc.2020.129491>

This is a PDF file of an article that has undergone enhancements after acceptance, such as the addition of a cover page and metadata, and formatting for readability, but it is not yet the definitive version of record. This version will undergo additional copyediting, typesetting and review before it is published in its final form, but we are providing this version to give early visibility of the article. Please note that, during the production process, errors may be discovered which could affect the content, and all legal disclaimers that apply to the journal pertain.

© 2020 Published by Elsevier B.V.

highlights

- Synthesis of new indolo[3,2-b]indoles via photooxidation and condensation have been reported.
- Photophysical properties of new indolo[3,2-b]indoles are explored and correlated experimental results with DFT.
- Indolo[3,2-b]indoles exhibited good hole mobility in organic thin-film transistor studies.

Journal Pre-proof

New Indolo[3,2-b]indole based small organic molecules for Organic Thin Film Transistors (OTFTs): A Combined Experimental and DFT Study

Venkat Swamy Puli,^b Mahesh Subburu,^a Bhongiri Yadagiri,^a Anuj Tripathi,^c K. R. S. Prasad,^b Anindita Chatterjee,^{b*} Someshwar Pola,^{a*} and Prabhakar Chetti^{c*}

^aDepartment of Chemistry, Osmania University, Hyderabad, India.

^bDepartment of Chemistry, Koneru Lakshmaiah Education Foundation, Vaddeswaram, Guntur, Andhra Pradesh, India.

^cDepartment of Chemistry, National Institute of Technology, Kurukshetra, India.

Abstract:

Synthesis of new indolo[3,2-b]indoles (**5a- 5j**) in presence of Ag-doped ZnO and (Diacetoxyiodo) benzene system under visible-light have been reported. All the new fused linear heterocyclic indolo[3,2-b]indole system (**5a- 5j**) thoroughly characterized by spectroscopic methods like mass, UV-visible, NMR and C, H, N elemental analysis. Further, their photophysical properties were carried out by combined experimental and theoretical studies. Thermogravimetric studies are carried out to confirm the thermal stability of molecules. The frontier molecular orbitals of molecules are characterized with the help of cyclic voltammetry. Additionally, the compounds of series **5** were used for the fabrication of organic thin-film transistors, which indicated the hole mobilities in the range of 0.11 – 0.85 cm²/Vs and with on/off ratio 10⁵ on ODTS-SiO₂ substrate at 50 °C and are also supported by DFT studies.

TO WHOM CORRESPONDENCE SHOULD BE ADDRESSED:

*Email: chetty_prabhakar@yahoo.com (P. Chetti); somesh.pola@gmail.com (S. Pola)

Introduction:

Recent advancement in the field of material chemistry shows that organic materials are the best alternative for inorganic ones. The major advantages of organic materials as semiconducting materials are low cost, light weight and they possess possibility of producing flexible and large area devices [1, 2]. These organic molecules find applications in different optoelectronic devices majorly in organic field-effect transistors (OFETs), organic photovoltaics (OPVs) and organic light-emitting diodes (OLEDs) [2-5]. Within organic molecules, π -conjugated organic framework finds application in organic semiconductors, some of them are well-reported in literature such as heteroacenes [6-7], polythiophenes [8- 9] oligoacenes [10-11], hexabenzocoronenes [12] and phthalocyanines [13-14]. Among different organic molecules mentioned above, acenes and heteroacenes are well explored by many researchers as they have high mobility, which is the key characteristic of organic semiconductor device. Within acenes, pentacene own high hole mobility of $5.0 \text{ cm}^2\text{V}^{-1}\text{s}^{-1}$ and is one of the most studied p-type materials [10,15]. However, these acenes i.e. pentacene was suffering from several shortcomings like air instability and low solubility under ambient conditions [16]. In order to overcome these shortcomings several strategies have been applied like substrate variation, functionalization of the molecular structure and introduction of heteroatom [17-18]. The structure of a molecule plays a key role in the molecular electronic approaches, since the molecular assemblies are in the solid-state, especially in the thin-film state, which directs intermolecular orbital overlap and advances the carrier/charge transport applications. Therefore, researchers are continuously focused on design and synthesis of new organic frameworks with better charge transport properties which find applications in optoelectronic devices. In context to this, here in this work it is focused on indolo[3,2-b]indole (**InIn**) as a promising π -core for a new type of organic semiconductors [19]. The rigid π -framework and planarity of **InIn** can help strong intermolecular interactions that would be appropriate for developing new organic semiconductor materials. The significant structural characteristics in **InIn** molecules is associated with a core structure of pyrrolo[3,2-b]pyrrole, which is fully π -extended molecular system and it offers high stability to the molecular system by lowering the HOMO energy levels [19]. These noticeable properties of pyrrolo[3,2-b]pyrrole have motivated organic chemists to develop new organic semiconductors with the pyrrolo[3,2-b]pyrrole structure in prolonged π -systems with more than one fused aromatic rings due to its π -extended structures [20-21].

The prominent π -structures of pyrrolo[3,2-b]pyrrole attracted us as a central core system for the synthesis of new organic molecules having applications in optoelectronic devices. For this, we concentrated on two indole systems fused together to give **InIn** and its derivatives with various small functional groups (molecule **5a-5j** in Figure1). The very first report on the synthesis of simplest system of **InIn** (**5a** in figure 1) was given by W. Treibs in 1961, but not fully characterized the synthesised molecule and its stability is also not clear [22]. Later, Hunig et al. in 1976 characterized **InIn** by Uv-vis and IR spectra [23]. Further, the stability of **InIn** was reported by Li Qui et. al. and is very stable in nature [19]. Recently Zeng et al reported about the stability of **InIn** and their derivatives, and they showed that the linear fusion of aromatic rings to the antiaromatic core increases the stability of heteroacenes [24]. By considering all the above facts, here in this paper, we report the synthesis of a series of **InIn** derivatives through insitu photooxidation-condensation reactions. The characterization of the synthesized **InIn** derivatives are done by means of C, H, N elemental analysis, mass, other spectral analysis, and their organic thin-film transistor (OTFT) features. The obtained results also supported with DFT studies.

Experimental Section:

Starting materials are purchased from Sigma-Aldrich such as various substituted nitrobenzenes, 2-iodo aniline, **AgNO₃**, **Zn(NO₃)₂** and other solvents and are used without further purification. 1,2-disubstituted-4-nitrobenzenes are converted into 3,4-disubstituted anilines using the reported procedure [25] and these anilines were reacted with N-iodosuccinimide to give 2-iodo-4,5-disubstituted anilines [26]. The detailed procedure for the synthesis of new photocatalysts and fused linear type heterocyclic compounds are presented in supporting information. The method for fabrication of the device for OTFTs and specific techniques are also shown in supporting information. Preparations of **Ag**-doped **ZnO** NPs are carried out by using the reported method [27].

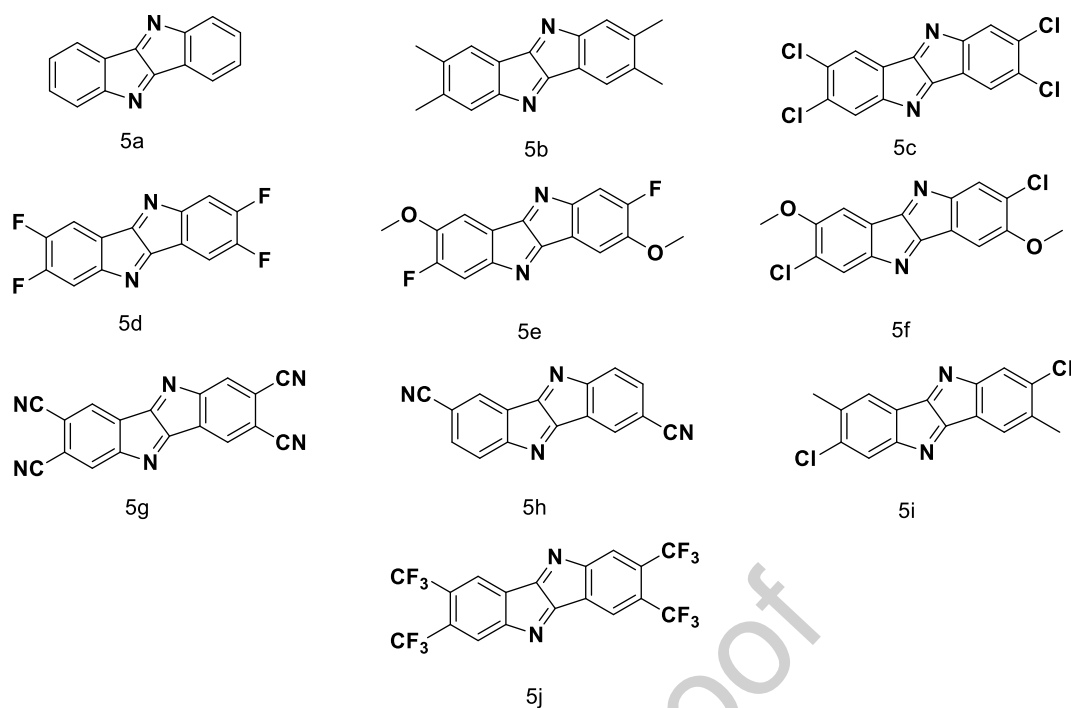
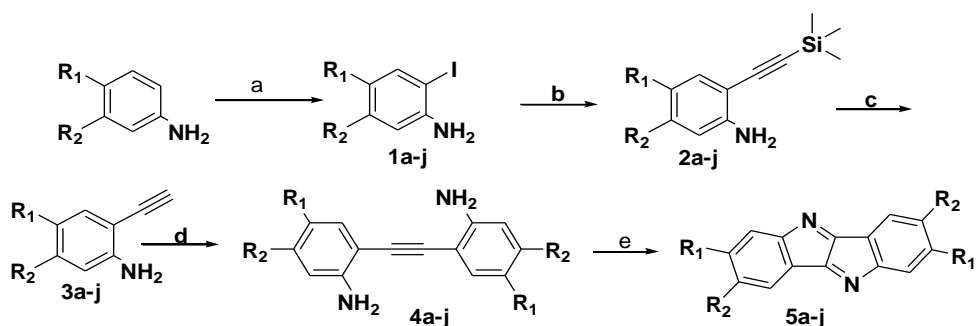


Fig.1. Structures of synthesized **InIn** and its derivatives (**5a-5j**)

General synthesis procedure:

The synthesis of new fused linear heteroacenes via photooxidation and condensation reactions in one-pot operation conditions is reported. Furthermore, the efficiency and sustainability of catalyst play a significant role in the catalytic properties [28]. Scheme 1 outlines the synthesis of indolo[3,2-b]indole and its derivatives from internal alkynes. The strategy is to synthesize various substituted 2-amino aryl iodides [29] **1a-j** and subsequent Sonagashira coupling reaction [30], followed by deprotection of the trimethylsilyl group for the formation of **2a-j**. The deprotection of **2a-j** yields terminal alkynes **3a-j**, which can further react with **1a-j** under Sonagashira coupling to obtain the corresponding internal alkynes **4a-j**. Further, the reaction of **4a-j** in the presence of Ag-doped ZnO and $\text{PhI}(\text{OAc})_2$ system under visible light irradiation was performed to get the desired product indolo[3,2-b]indoles **5a-j** (table 1). Detailed synthetic procedure of each step and spectral data is provided in supporting information).



a) NIS, acetic acid, rt, 5h; b) ethynyltrimethylsilane, Pd(PPh₃)₂Cl₂, Cul, triethylamine, toluene, reflux; c) K₂CO₃, methanol, rt; d) compounds (1a-j), Pd(PPh₃)₂Cl₂, PPh₃, Cul, triethylamine, toluene, reflux; e) Ag-doped ZnO NPs, PhI(OAc)₂, H₂O and CH₃CN (1:1), hν.

Scheme 1: Synthesis of indolo[3,2-b]indole and its derivatives

Table 1: Synthesis of new indolo[3,2-b]indole derivatives with different functional groups and their %yield

Substituents	Product	%Yield
R ₁ =R ₂ = -H	5a	86
R ₁ =R ₂ = -CH ₃	5b	71
R ₁ =R ₂ = -Cl	5c	66
R ₁ =R ₂ = -F	5d	59
R ₁ =-OCH ₃ ; R ₂ = -F	5e	68
R ₁ = -OCH ₃ ; R ₂ =-Cl	5f	65
R ₁ =R ₂ = -CN	5g	58
R ₁ = -CN; R ₂ = -H	5h	52
R ₁ = -CH ₃ ; R ₂ = -Cl	5i	69
R ₁ =R ₂ = -CF ₃	5j	54

Organic field effect transistors (OFETs) characteristics:

Bulky-Area Crystalline Films Placed on SiO₂ for compounds **5** series. The silicon wafers, with 200 nm thermally grown oxide layer, were cleaned by Piranha solution and rinsed thoroughly with ultra-high purity water. The cleaned silicon wafers were soaked into 1% *n*-

octadecyltrichlorosilane (ODTS) solution in dry toluene for 3 minutes to generate the ODTS-modified silicon oxide surface (ODTS-SiO₂/Si). Thin films of compound **5** series were thermally evaporated under a vacuum of 1×10^{-5} torr and deposited on SiO₂/Si or ODTS-SiO₂/Si coatings at different substrate temperatures (Figure 2) [31]. FET devices were fabricated with the 200 nm-thick SiO₂ surfaces as the gate dielectric and the highly *n*-doped silicon wafer as the gate electrode. The 50 nm-thick gold source and drain electrodes were deposited on the organic films (top contact) through a shadow mask. The channel length (*L*) and width (*W*) are 50 μm and 500 μm respectively.

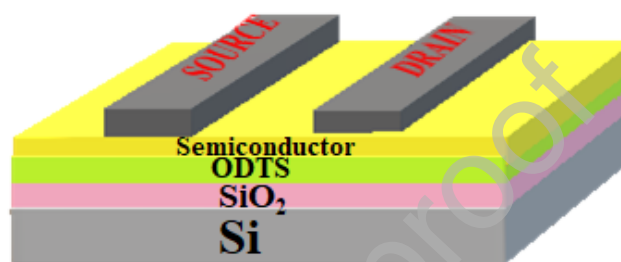


Fig.2: Schematic device structure

Characterization of Indolo[3,2-b]indole derivatives and device fabrication

All the photoreactions were performed by using a multi-tube photo-reactor system with LED visible light, Lelesil Innovative Systems, India. Mass spectral data collected by HR-EI systems on JMS-700 double-focusing mass spectrometer (JEOL, Tokyo, Japan). ¹H and ¹³C-NMR spectra recorded on a Bruker AV400 MHz Spectrometer with chemical shifts referenced using the ¹H resonance of residual CDCl₃ and d₆-DMSO. C, H, N, F and Cl elemental analysis have been carried out by using Elemental Analyzer Flash EA 1112. Melting points verified on a Cintex apparatus. Cyclic voltammetry measurements were conducted on a PC-controlled CHI 62C electrochemical analyser in a C₂H₄Cl₂ solvent at a scan rate of 100mVs⁻¹ using tetrabutylammonium perchlorate (0.1 M) as the supporting electrolyte. The glassy carbon, standard calomel electrode (SCE) and platinum wire were used as working, reference and counter electrodes, respectively. The electronic spectra obtained in chloroform solutions on a JASCO V-650 UV-Vis spectrophotometer. The AFM imaging was achieved on KeySight 5500 instrument (Agilent Technologies) underneath tapping mode with silicon nitride tip. Electrical characteristics were recorded under dark in air using a semiconductor device analyzer (Agilent-B-1500A). The mobility and threshold

voltage were taken out from transfer characteristics in the saturated regime by using the following equation:

$$I_d = \frac{W}{2L} \mu_{sat} C_i (V_g - V_{th})^2$$

Where W and L are the channel width and length respectively, and C_i is the capacitance per unit area of the SiO_2 insulator, V_g is the gate voltage, and V_{th} is the threshold voltage.

Results and Discussions:

Absorption and emission properties:

The **InIn** derivatives exhibits lemon yellow to bronze colour in their solid states (colour of the solid compounds shown in figure S1). Initially, the UV-vis absorption spectra of the compound **5a** recorded in dilute dichloroethane (DCE) solution as a function of time, are revealed in Figure S2. After 24 hours, no transformation in the electronic spectra was observed. The absorption spectra of all **InIn** derivatives as verified in dilute DCE solution are shown in Figure S3a-S3d and associated data are summarized in Table 2. Fused hetero-aromatic molecules are recognized to have robust, visible absorption and strong emission with competent quantum yields [32-33]. The absorption maxima for all the molecules are in the range of 433 nm to 477 nm with high molar extinction coefficients in DCE (Table 2). The red-shift tendency of the absorption maximum was noticed when the compound substituted with electron-donating group (**5b**, **5e**, **5f** and **5i**) as compared with the parental compound **5a** (Figure S3a). With the substitution of electron-withdrawing group on **InIn** (**5c**, **5d**, **5g**, **5h** and **5j**), results in blue-shifted absorption maxima (Figure S3b).

The absorption maxima of compounds **5a-5j** in the solid phase were significantly shifted to a higher wavelength region compared to its solution state (Table 2). The absorption maximum of **5b** is shifted from 472 nm in DCE to 582 nm in the solid phase, ensuing in a wavelength shift of 110 nm. The excitation maximum of **5e** is also shifted from 473 nm in DCE to 591 nm in the solid phase, ensuing in a 118 nm shift towards higher wavelength side. Compound **5b** and **5e** show the most substantial red-shift in the solid phase, while compounds **5i** and **5f** show the smallest wavelength shift in the solid-state (Table 2). Based on these outcomes, it is presumed that the shift towards higher wavelength region in the excitation maxima in its solid phase for compounds **5a-5j** is because of the compressed molecular arrangement in the solid phase and non-covalent interactions form its π - π assembly [34]. These π - π interactions

generate a distended system of conjugation in the solid phase, ensuing in the high wavelength shifts in the solid phase as related to the solution outcomes.

Table 2: Experimental UV-visabsorption (λ_{\max}) and molar extinction coefficient (ϵ) for the compounds **5a-5j** in DCE and absorption in solid-state ($\lambda_{\max-SS}$)

Material	λ_{\max} (nm)	ϵ L mol ⁻¹ cm ⁻¹	$\lambda_{\max-ss}$ (nm)
5a	465	58125	523
5b	472	59000	582
5c	446	55750	508
5d	441	55125	523
5e	473	59125	591
5f	470	58750	519
5g	434	54250	506
5h	433	54125	510
5i	477	59625	504
5j	436	54500	517

To advance understanding into the experimental electronic excitations of the molecules, DFT and TD-DFT calculations have been carried out for **5a-5j**. The ground state molecular geometries of **5a-5j** are fully optimized without any symmetric considerations in gas phase by using Gaussian 09 software [35] with DFT method at B3LYP level in combination with the basis set 6-31G (d, p). There is no imaginary frequency in the calculated vibrational spectrum of all the optimized structures, which indicates that all the optimized structures are located at the least point of the potential surface. TD-B3LYP method with 6-31G (d, p) basis set is used to get electronic absorption properties for the optimized geometries, and frontier molecular orbitals were pictorially visualized from the population analysis at same level of theory.

Computed excitations are in good agreement with the experimentally determined excitation energies. The calculated absorption maxima for all the molecules are in the range of 448 nm–498 nm. The calculated lowest three excitation energies, oscillator strengths, significant transitions, and percentage configuration interactions (% Ci) for molecules **5a-5j** are shown in Table S1. In all the molecules, the lowest excitation energy is with low intensity, the second and third excitation energies are with high intensities. For all the molecules (except molecule **5c** and **5e**), low-intensity absorption is due to the transition among HOMO-2 to LUMO. In the case of molecules **5c** and **5e**, the first excitation with low intensity is from HOMO-3 to LUMO. The corresponding frontier molecular orbitals for molecule **5a**, are

shown in **Figure 3**. The second excitation in all the molecules (except **5e**) is due to the transition between HOMO-1 to LUMO.

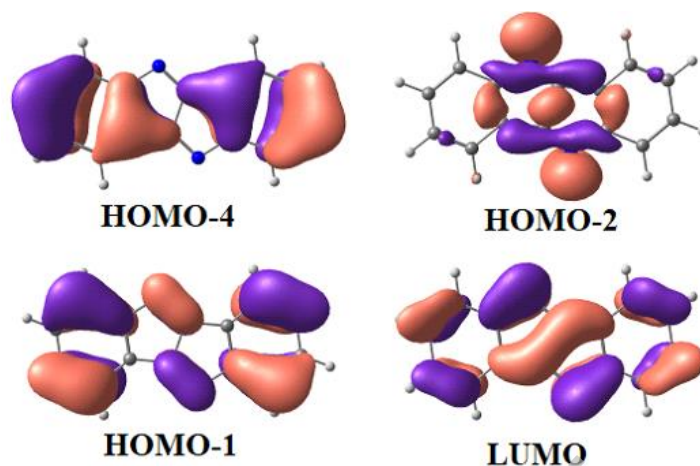


Fig. 3: Molecular orbital pictures for molecule 5a

The fluorescence spectra of molecules **5a-5j** are measured against tetracene as a typical reference. Table 3 displays the emission maxima and the quantum yields of all the fused hetero-aromatic molecules in DCE and the emission maxima in the solid-state. In solution state, the compounds **5b**, **5e**, and **5i** show emission intensity approximately twice than that of **5a** (Figure S4). However, the quantum yield of all the compounds is in the range of 0.21 to 0.51 (Table 3), comparable to that of compound **5a**.

For all the molecules **5a-5j**, the emission maxima were moved to a higher wavelength region in its solid phase. In the case of compound **5h**, exhibited the higher change in emission maxima from 479 nm in DCE to 608 nm in the solid phase, ensuing in a wavelength difference is 129 nm (Table 3). The maximum change in wavelength was observed in compounds **5g** and **5h**, whereas a marginal shift of wavelength noticed in compounds **5d** and **5i**. The more compressed molecular arrangements in the solid phase can outcome in π - π assemblies and endorse a change of emission maxima [34, 36].

Table 3 Emission λ_{\max} and quantum yield for compounds **5a-5j** in DCE and in the solid state

Material	λ_{\max} (nm)	Φ_F	Solid-state excitation
			λ_{\max} (nm)
5a	536	0.37	655
5b	544	0.46	658
5c	489	0.49	607
5d	485	0.35	587
5e	539	0.42	652
5f	536	0.44	654
5g	489	0.51	612
5h	479	0.29	608
5i	552	0.55	655
5j	480	0.21	603

HOMO-LUMO Energies and Thermal Properties:

The HOMO and LUMO energy levels are measured by cyclic voltammetry (CV) in DCE (Cyclic voltammograms are shown in Figure 4). The oxidation potentials along with the HOMO and LUMO energy levels obtained from CV of compounds **5a** to **5j**, presented in Table 4. The ranges of oxidation potentials for all the reported compounds are from 1.24 to 1.46 V. The measured HOMO levels of all the molecules are in the range of -5.85 to -5.62 eV; similarly, the LUMO energies are in the range of -3.09 to -2.81 eV. Further, HOMO-LUMO energies are also calculated by DFT methodology at the B3LYP method. The calculated HOMO and LUMO energies are also tabulated in Table 4. All the calculated HOMO, LUMO energy levels are comparable with the experimentally determined energies (following the trend). All these HOMO levels are lesser than that of tetracene (-4.85eV) [37]. It may have to do with the electronegative groups present in the molecular framework, even though indole rings are fused. The lower HOMO levels suggest that all these compounds are more stable against oxidation. The optical band gaps of these compounds (**5a-5j**) are obtained from the absorption edges of their UV-visible spectra. LUMO energies are evaluated through two methods, one is subtracting the optical band gap values from HOMO values and another method is reduction potentials of CV. From both the techniques LUMO energies are almost similar. With the substituent electron donating / withdrawing groups are responsible for the small variation in observed in LUMO values [38]. Compounds **5a-5j** showing $1e^-$ irreversible oxidation peaks, which corresponds to the electron-rich indole moiety. These are also showing multiple oxidation peaks that could originate from indole moiety and the

corresponding voltammograms are shown in Figure 4 [38]. HOMO energy levels of compound **5a–5j** are calculated from the onsets of the oxidation peaks observed in the CV analysis (Table 4).

Table 4: Measured optical band gap, oxidation potentials, HOMO-LUMO energies and DFT calculated HOMO-LUMO gap along with HOMO-LUMO energies

Compound	E_{oxd} (V) ^a	E_{HOMO} (eV) ^a	E_{LUMO} (eV) ^a	$E_{\text{g}}^{\text{opt}}$ (eV) ^a	E_{HOMO} (eV) ^b	E_{LUMO} (eV) ^b	$E_{\text{g}}^{\text{opt}}$ (eV) ^b
5a	1.43	-5.82	-2.89	2.93	-6.02	-3.10	2.92
5b	1.38	-5.79	-2.96	2.83	-5.60	-2.82	2.78
5c	1.37	-5.76	-3.01	2.75	-6.49	-3.78	2.71
5d	1.46	-5.85	-3.09	2.76	-6.25	-3.56	2.69
5e	1.31	-5.62	-3.01	2.61	-5.58	-2.99	2.59
5f	1.24	-5.63	-3.08	2.55	-5.67	-3.17	2.50
5g	1.29	-5.68	-3.01	2.67	-7.57	-4.85	2.72
5h	1.41	-5.80	-3.02	2.78	-6.90	-4.06	2.84
5i	1.28	-5.67	-2.88	2.79	-6.08	-3.33	2.75
5j	1.33	-5.75	-2.81	2.94	-7.20	-4.24	2.96

^aDetermined from CV and ^bDFT-Calculated energies

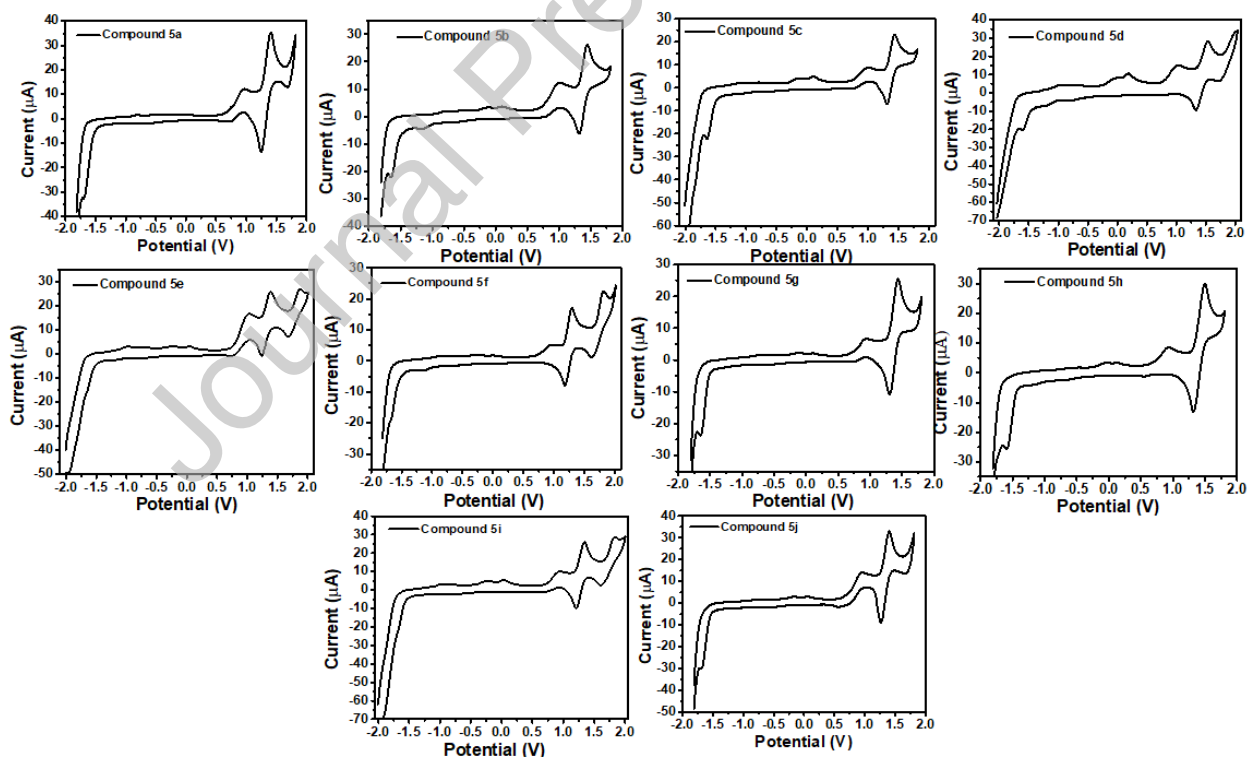


Fig. 4: Cyclic voltammograms for compounds **5a – 5j**

All the reported compounds are analyzed for their thermal properties. Measured melting points and decomposition temperatures are presented in Table 5. Thermo-gravimetric plots of compounds **5a-5j** are shown in Figure S5. All the compounds exhibit high-thermal stability,

decomposing at >300 °C and the compound **5d** with four fluorine atoms retains highest T_d . Such high thermal stability of these molecules gives a clear indication that these were less prone to thermal degradation. This particular feature has significance in the utility of these materials in device properties.

Table 5 Melting point (M.P in °C) and decomposition temperature (T_d in °C) of compound 5 series

Mol	5a	5b	5c	5d	5e	5f	5g	5h	5i	5j
M.P	256- 258	232- 234	324- 326	297- 301	286- 288	291- 293	331- 333	276- 278	288- 290	341- 343
T_d	331	318	392	383	376	389	381	366	378	402

Thin film deposition:

All the compounds of **5** series were fabricated for the thin film transistor devices and mobility data shown in Table 6. The AFM image of 50 nm dense film of compound **5a** and **5b** are shown in Figure 5a-d. In the case of the AFM image of 50 nm dense films, the compound **5a** and **5b** are placed on **ODTS-SiO₂**, and **SiO₂** surfaces at various temperatures. The same substrate temperatures were utilized throughout the process of deposition. Grains size of molecules on **ODTS**-modified **SiO₂** surface was bigger than placed on un-modified **SiO₂** surface at a substrate temperature of 25°C and 50°C. Films of compound **5a** and **5b** placed at a substrate temperature 50° C provides the smaller grain size of **SiO₂** surface but on **ODTS** modified **SiO₂** surface largest grain size and fine terrace structure [39]. Figure S6a exhibits the powder X-ray diffraction of thin-films of compound **5a** placed on **SiO₂** and **ODTS-SiO₂** surfaces at various temperatures. Diffraction pattern has the peaks such as 2θ at 5.9854°, 12.042° and 16.337° are obtained at all substrates temperature and are assigned as the diffractions from (001), (002), (003) planes correspondingly. This designates a similar crystal phase at various conditions of deposition. The d-spacing value obtained from (001) peak is 151.9 Å, equated to the determined length of 149.6 Å, signifying molecules were vertical near standing on all surfaces [40]. This alignment will enable charge-transporting facility in a flat device arrangement subsequently the path of π - π assembling of the brick-wall or co-facial prearrangement equals the conduction pathway. In the diffractograms of compound **5a** the intensity of the diffracted peaks on different surfaces and substrate temperatures corresponded with mobility. Peak intensities are higher for the films grown on **SiO₂**, and **ODTS** modified surfaces at all substrate temperatures. The thin-film is produced on the **SiO₂/Si** surface with the substrate temperature at 50 °C peak intensity higher than room

temperature and at 80°C. Figure S6b shows films of compound **5b** placed on **SiO₂** and **ODTS-SiO₂** at various temperatures. Another time, a single crystalline phase showing diffraction peaks at 2θ of $6.488^\circ(001)$, $12.68^\circ(002)$, $17.14^\circ(003)$ correspondingly were attained at non-identical substrate temperature. The d-spacing value obtained from (001) is 145.1 Å which also specifies a vertical alignment of compound **5b** on the surfaces.

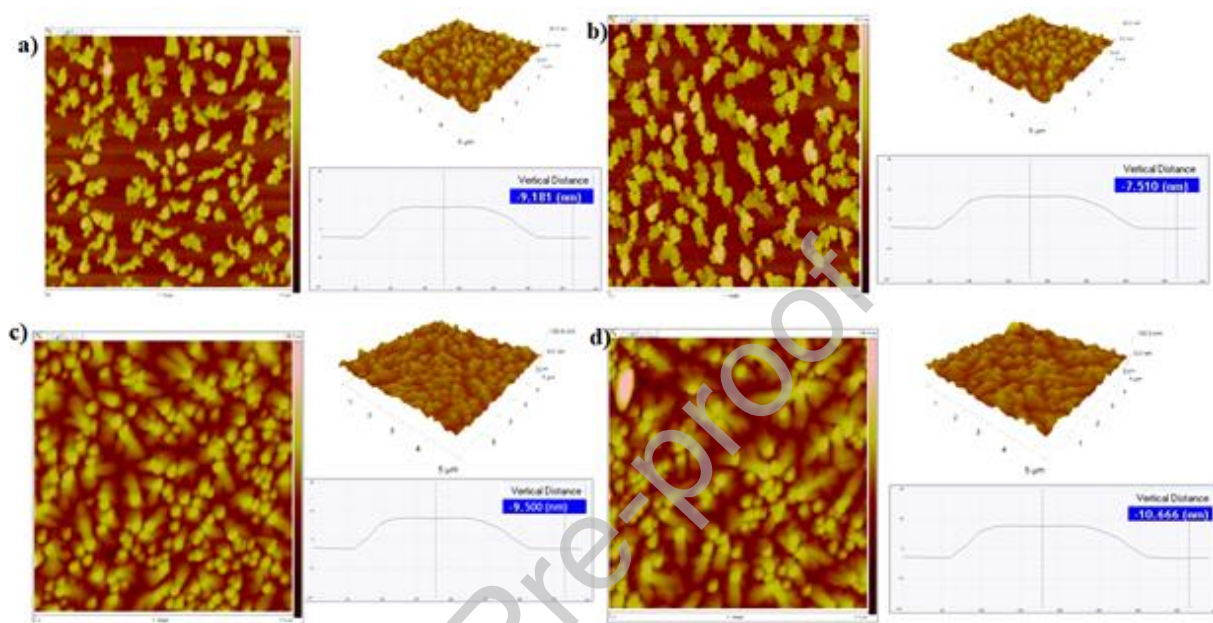


Fig.5: AMF images of ODTS on **SiO₂** substrate a) compound **5a** at 25 °C, b) compound **5a** at 50 °C, c) compound **5b** at 25 °C, and d) compound **5d** at 50 °C

Characteristics of FET devices [2] prepared from compound **5a**, and compound **5b** are shown in Table 6 with the corresponding curves (**Figure 6a-d**). For compound **5a**, the top device performance was attained for the film placed on **ODTS** modified surface at a substrate temperature of 50°C, the highest mobility $0.49 \text{ cm}^2/\text{Vs}$ is on surface-modified (**ODTS-SiO₂**) at 50°C. The mobility reduced with smaller substrate temperatures. This tendency also matches the result from AFM analysis, the bigger the grain size, and then the mobility is higher. The film placed on **ODTS-SiO₂** surface has the maximum mobility is $0.12 \text{ cm}^2/\text{Vs}$ which was attained at 25°C has deposition conditions.

Additionally, enhancing the substrate temperature leads to decrease in intensity of diffraction peaks and lower device performance. For compound **5b**, the foremost execution was captured on **ODTS-SiO₂** surface at 25°C deposition conditions. The mobility of $0.28 \text{ cm}^2/\text{Vs}$ and an on/off ratio up to 10^4 were reached. For compound **5b**, the foremost device execution was attained for the film placed on **ODTS-SiO₂** modified surface at the substrate temperature of

50°C [31] and obtained the highest mobility 0.85 cm²/Vs. Advanced deposition temperatures significantly dropped in the mobility of all surfaces. All the molecules show transistor property and the mobility data presented in Table 6.

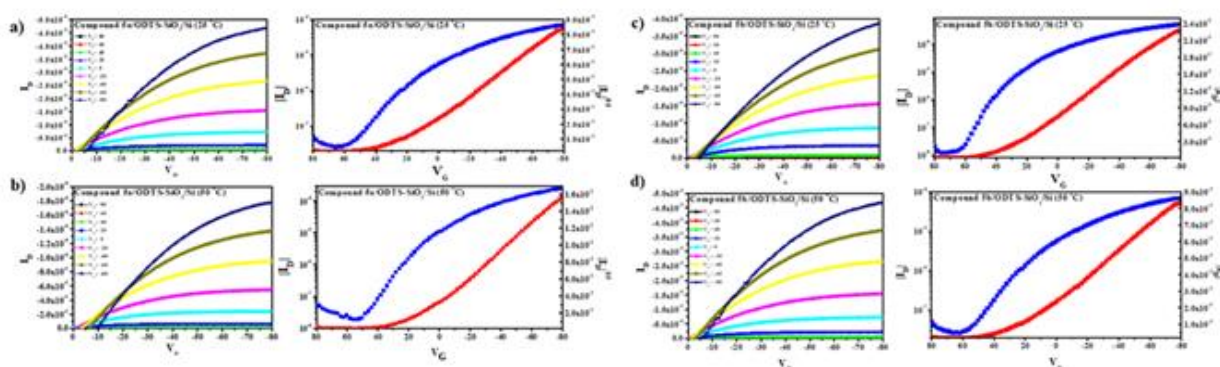


Fig. 6: I-V curves of OFET various temperatures on ODTS-SiO₂ substrates a) compound **5a** on ODTS-SiO₂ at 25 °C; b) compound **5a** on ODTS-SiO₂ at 50 °C, c) compound **5b** on ODTS-SiO₂ at 25 °C; and d) compound **5b** on ODTS-SiO₂ at 50 °C

Table 6: Electric characteristics of compounds **5a–5j** OFETs on ODTS-SiO₂ substrate at various temperatures

Compound	Mobility (cm ² /Vs) at 25 °C (50 °C)	I _{on} /I _{off} current ratio at 25 °C (50 °C)
5a	0.12 (0.49)	10 ⁴ (10 ⁵)
5b	0.28 (0.85)	10 ⁴ (10 ⁵)
5c	0.21 (0.53)	10 ⁴ (10 ⁴)
5d	0.14 (0.35)	10 ⁴ (10 ⁴)
5e	0.16 (0.30)	10 ⁴ (10 ⁴)
5f	0.11 (0.19)	10 ⁴ (10 ⁴)
5g	0.13 (0.21)	10 ⁴ (10 ⁴)
5h	0.15 (0.24)	10 ⁴ (10 ⁴)
5i	0.08 (0.18)	10 ⁴ (10 ⁴)
5j	0.06 (0.11)	10 ⁴ (10 ⁴)

Reorganization energies:

Further, to get insight into the mobility in these molecules, we have also calculated reorganization energies by using DFT methods. It is well known that mobility and

reorganization energy are inversely proportional to each other i.e. smaller reorganization energy lead to higher mobility of molecule.

According to Marcus Hopping model, the rate constant for charge transfer reaction is given by [41-42]

$$K = \left(\frac{4\pi^2}{h}\right) H^2 (4\pi\lambda kT)^{-1/2} \exp\left(-\lambda/4kT\right) \dots \dots \dots 1$$

Here, K and k_b are rate constant and Boltzmann constant respectively. T , λ and ΔH are absolute temperature, reorganization energy and charge transfer integral matrix element between neighbouring molecule respectively [43]. It is clear from the above equation that rate constant (K) is inversely proportional to reorganization energy of the molecule. Further, reorganization energies are characterized into external and internal λ which are mainly imparted from surrounding medium and intramolecular vibrations respectively. In comparison to internal reorganization energies external reorganization energies are very little and hence can be neglected [44]. Here we calculated internal reorganization energy for hole (λ_h) and electron (λ_e) using equations 2a and 2b respectively [45-46].

$$\lambda_h = (E_n^+ - E^+) + (E_+^n - E^n) \dots \dots \dots 2a$$

$$\lambda_e = (E_n^- - E^-) + (E_-^n - E^n) \dots \dots \dots 2b$$

In the above-mentioned equation, E^n , E^- and E^+ represents the energies of neutral, anion and cation molecules in its lowest energy geometries, respectively. E_n^- (E_n^+) represents energies of anion (cation) molecule obtained at optimized ground state of the neutral molecule. E_-^n (E_+^n) represents the energy of neutral molecule obtained at optimized anionic (cationic) state.

The calculated hole (λ_h) and electron (λ_e) reorganization energies are given in Table 7. The molecules like **5a**, **5b**, **5c**, **5g**, **5h**, **5i**, and **5j** are showing comparable or smaller λ_h value than the standard hole-transporting material N,N'-diphenyl-N,N'-bis(3-methylphenyl)-(1,1'-biphenyl)-4,4'-diamine (TPD, $\lambda_h=290$ meV) [47]. Further, the calculated λ_e values are above 400 meV which is not good for electron transport material. For all the molecules $\lambda_h < \lambda_e$, means studied molecules are better for hole transporting material which is also confirmed by experimental results. In conclusion these the molecules can be used for hole transporting material rather than electron transporting material.

Table 7: Calculated hole (λ_h) and electron (λ_e) reorganization energy (in meV)

Compound	5a	5b	5c	5d	5e	5f	5g	5h	5i	5j
$\lambda_h \rightarrow$	282	269	287	361	391	348	206	230	288	398
$\lambda_e \rightarrow$	474	471	491	545	781	748	409	473	492	592

Conclusions:

The reaction proceeds in the presence of Ag-doped ZnO with PhI(OAc)₂ conditions to generate polycyclic fused linear heterocycles by using a broad range of substrates under visible light irradiation. In the process of photooxidation and condensation of various 2,2'-(ethyne-1,2-diyl)dianilines converted to indolo[3,2-b]indoles. Indolo[3,2-b]indole and its derivatives have exhibited good optical properties and the shifting of absorption bands depends upon dipole groups, and also shown good correlation between experimental and DFT calculations. All the compounds are showing high-thermal stability, decomposing at >300 °C, which gives a clear indication that these were less prone to thermal degradation and this particular feature is significant in device properties. The compounds **5a-5j** used for organic thin-film transistors studies and preliminary results shows the hole mobility in the range of 0.11- 0.85 cm²/Vs and with on/off ratio 10⁴-10⁵ respectively. The calculated hole reorganization energies are smaller than electron reorganization energies and these are good for hole transporting material.

Credit author statement

Methodology, Investigation, Formal analysis and Writing – original draft by Venkatswamy Puli, Mahesh Subburu, Anuj Tripathi, Yadagiri Bhongiri, K. R. S. Prasad, and Anindita Chatterjee.

Conceptualization, Software, Validation, Formal analysis, Resources, Writing – review and editing, Supervision and Project administration by Dr. Someswar Pola and Dr. Prabhakar Chetti.

Prabhakar Chetti

Declaration of interests

The authors declare that they have no known competing financial interests or personal relationships that could have appeared to influence the work reported in this paper.

Prabhakar Chetti

Supporting Information

UV-visible and emission spectra and thermograms of compounds **5a** to **5j** are presented in supporting information part. P-XRD images of thin films, spectral data such as $^1\text{H-NMR}$, $^{13}\text{C-NMR}$, Mass spectra and CHN elemental analysis are also supported in supporting information.

Acknowledgement

SP and CP thanks to SERB - New Delhi, India under EMR (EMR/2014/000452) and CSIR- New Delhi (02(0339)/18/EMR-II) respectively for financial support. Special appreciations to DST-FIST, New Delhi. We also thankful to Prof. Yu-Tai Tao, Institute of Chemistry, Academia Sinica, Taipei, Taiwan and Dr. V. J. Rao, CSIR-IICT, Hyderabad, India.

References:

1. S.R. Forrest, *Nature* 428 (2004) 911-918.
2. M.M. Torrent, C. Rovira, *Chem. Rev.* 111 (2011) 4833-4856.
3. Q-D. Liu, R-X. Peng, S-J. Chen, L. Ai, S-Y. Wang, Z-Y. Liu, Z-Y. Ge, *Macromol. Chem. Phys.* 215 (2014) 1287-1296.
4. M. Nakano, K. Niimi, E. Miyazaki, I. Osaka, K. Takimiya, *J. Org. Chem.* 77 (2012) 8099-8111.
5. S. Arulmozhiraja, T. Ohno, *J. Phys. Chem. C*, 112 (2008) 16561-16567.
6. M. J. Kang, I. Doi, H. Mori, E. Miyazaki, K. Takimiya, M. Ikeda, H. Kuwabara, *Adv. Mater.*, 23 (2011) 1222-1225.
7. S. Shinamura, I. Osaka, E. Miyazaki, A. Nakao, M. Yamagishi, J. Takeya, K. Takimiya, *J. Am. Chem. Soc.*, 133 (2011) 5224-5035.
8. J. Roncali, *Chem. Rev.*, 92 (1992) 711-738.
9. I. F. Perepichka, D. F. Perepichka, H. Meng, F. Wudl, *Adv. Mater.*, 17 (2005) 2281-2305.
10. J. E. Anthony, *Chem. Rev.*, 106 (2006) 5028-5048.
11. J. E. Anthony, *Angew. Chem., Int. Ed.*, 47 (2008) 452-483.
12. J. Wu, W. Pisula, K. Mullen, *Chem. Rev.*, 107 (2007) 718-747.
13. Z. Bao, A. J. Lovinger, J. Brown, *J. Am. Chem. Soc.*, 120 (1998) 207-208.
14. J. G. Xue, S. Uchida, B. P. Rand, S. R. Forrest, *Appl. Phys. Lett.*, 85 (2004) 5757-5759.

15. T.W Kelley, D.V. Muires, P.F. Baude, T.P. Smith, T.D. Jones, *Mater. Res. Soc. Symp. Proc.* 771 (2003) L6.5.1.
16. P. Coppo, S. G. Yeates, *Adv. Mater.* 17 (2005) 3001-3005.
17. P. K. De, D. C. Neckers, *Org. Lett.* 14 (2012) 78-81.
18. M. M. Payne, S. R. Parkin, J. E. Anthony, *J. Am. Chem. Soc.* 127 (2005) 8028-8029.
19. L. Qiu, X. Zhuang, N. Zhao, X. Wang, Z. An, Z. Lan, X. Wan, *Chem. Commun.*, 50 (2014) 3324-3327
20. K. Takimiya, T. Yamamoto, H. Ebata, T. Izawa, *Adv. Mater.*, 8(2007) 273-276.
21. K. Takimiya, S. Shinamura, I. Osaka, E. Miyazaki, *Adv. Mater.*, 23 (2011) 4347-4370.
22. W. Treibs, *Naturwissenschaften*, 48 (1961) 130
23. S. Hünig and H.-C. Steinmetzer, *Justus Liebig's Ann. Chem.*, (1976) 1090-1102
24. J. Zheng, X. Zhuang, L. Qiu, Y. Xie, X. Wan, Z. Lan, *J. Phys. Chem. A*, 2015, 119, 3762-3769.
25. M. Orlandi, F. Tosi, M. Bonsignore, M. Benaglia, *Org. Lett.*, 17 (2015) 3941.
26. M. C. Carrefio, J. L. G. Ruano, G. Sanz, M. A. Toledo, A. Urbano, *Tetrahedron Lett.*, 37 (1996) 4081.
27. R. J. V. Michael, B. Sambandam, T. Muthukumar, M. J. Umapathy, P. T. Manoharan, *Phys. Chem. Chem. Phys.*, 16 (2014) 8541.
28. M. Machida, X.W. Ma, H. Taniguchi, J. Yabunaka, T. Kijima, *J. Mol. Catal. A: Chem.*, 155 (2000) 131.
29. A. R. Hajipour, M. Arbabian, A. E. Ruoho, *J. Org. Chem.*, 67 (2002) 8622.
30. A. B. Lemay, K. S. Vulic, W. W. Ogilvie, *J. Org. Chem.*, 71 (2006) 3615.
31. F. Valiyev, W.-S. Hu, H.-Y. Chen, M.-Y. Kuo, I. Chao, Y.-T. Tao, *Chem. Mater.*, 19 (2007) 3018.
32. S. Pola, Y. Bhongiri, R. Jadhav, P. Chetti, G. Venkanna, *RSC Adv.*, 6 (2016) 88321.
33. C. J. S. Louis, L. L. Magill, J. A. Wilson, A. R. Schroeder, S. E. Harrell, N. S. Jackson, J. A. Trindell, S. Kim, A. R. Fisch, L. Munro, V. J. Catalano, C. E. Webster, P. P. Vaughan, K. S. Molek, A. K. Schrock, M. T. Huggins, *J. Org. Chem.*, 81 (2016) 10955.
34. J. Grolleau, R. Petrov, M. Allain, W. G. Skene, P. Frere, *ACS Omega*, 3 (2018) 18542.
35. M. J. Frisch, G. W. Trucks, H. B. Schlegel, G. E. Scuseria, M. A. Robb, J. R. Cheeseman, G. Scalmani, V. Barone, B. Mennucci, G. A. Petersson, H. Nakatsuji,

- M. Caricato, X. Li, H. P. Hratchian, A. F. Izmaylov, J. Bloino, G. Zheng, J. L. Sonnenberg, M. Hada, M. Ehara, K. Toyota, R. Fukuda, J. Hasegawa, M. Ishida, T. Nakajima, Y. Honda, O. Kitao, H. Nakai, T. Vreven, J. A. Montgomery, Jr., J. E. Peralta, F. Ogliaro, M. Bearpark, J. J. Heyd, E. Brothers, K. N. Kudin, V. N. Staroverov, R. Kobayashi, J. Normand, K. Raghavachari, A. Rendell, J. C. Burant, S. S. Iyengar, J. Tomasi, M. Cossi, N. Rega, J. M. Millam, M. Klene, J. E. Knox, J. B. Cross, V. Bakken, C. Adamo, J. Jaramillo, R. Gomperts, R. E. Stratmann, O. Yazyev, A. J. Austin, R. Cammi, C. Pomelli, J. W. Ochterski, R. L. Martin, K. Morokuma, V. G. Zakrzewski, G. A. Voth, P. Salvador, J. J. Dannenberg, S. Dapprich, A. D. Daniels, O. Farkas, J. B. Foresman, J. V. Ortiz, J. Cioslowski, and D. J. Fox, Gaussian 09, Revision E.01, Gaussian, Inc., Wallingford CT, (2013).
36. K. Ono, H. Yamaguchi, K. Taga, K. Saito, J. Nishida and Y. Yamashita, *Org. Lett.*, 11 (2009) 149.
37. K. Takimiya, T. Yamamoto, H. Ebata, T. Izawa, *Sci. Tech. Adv. Mater.*, 8(2007) 273-276.
38. Y-T. Tao, S. Pola, S. Kumar, M. M. Islam, *J. Org. Chem.*, 82 (2017) 8067.
39. F. Dai, X. Liu, T. Yang, J. Qian, Y. Li, Y. Gao, P. Xiong, H. Ou, J. Wu, M. Kanehara, T. Minari, C. Liu, *ACS Appl. Mater. Inter.*, 11 (2019) 7226.
40. Y. Wen, Y. Liu, Y. Guo, G. Yu, W. Hu, *Chem. Rev.*, 111(2011) 3358.
41. R. A. Marcus, N. Sutin, *Biochim. Biophys. Acta*, 811 (1985) 265.
42. K. V. Mikkelsen, M. A. Ratner, *Chem. Rev.*, 87 (1987) 113.
43. S. F. Nelsen, F. Blomgren, *J. Org. Chem.*, 66 (2001) 6551.
44. D. P. McMahon, A. Troisi, *J. Phys. Chem. Lett.*, 1 (2010) 941.
45. A. Tripathi, C. Prabhakar, *J. Phys. Org. Chem.*, 32 (2019) e3944.
46. A. Tripathi, C. Prabhakar, *J. Mol. Struct.*, 1203 (2020) 127397.
47. M. Malagoli, J. L. Bredas, *Chem Phys. Lett.* 327 (2000) 13-17.